Hindawi
Geofluids
Volume 2022, Article ID 6821810, 13 pages
https://doi.org/10.1155/2022/6821810

Research Article

Impact of Depressurizing Boreholes on Energy Dissipation in Deep Roadway

Meng Wang,[1,2] Zhixue Li,[1] Yalong Xu,[1] Zhenhua Li,[1] Ruifu Yuan,[1] Hongchao Zhao,[3] and Guodong Li[3]

[1]*School of Energy Science and Engineering, Henan Polytechnic University, Jiaozuo, China*
[2]*State Collaborative Innovation Center of Coal Work Safety and Clean-Efficiency Utilization, Jiaozuo, China*
[3]*School of Geology and Mining Engineering, Xinjiang University, Urumchi, China*

Correspondence should be addressed to Yalong Xu; yalong_xu2021@126.com

Received 8 March 2022; Accepted 28 June 2022; Published 16 July 2022

Academic Editor: Jianyong Han

Depressurizing borehole drilling is an effective approach to control the large deformation of deep roadway. It can transfer the high stress in the proximity of the roadway into the deep stable rock masses. However, it should be noted that the borehole drilling will inevitably cause the secondary damage to roadway. To determine the parameters of depressurizing boreholes, the degree of the secondary damage must be evaluated properly. Given that the rock mass failure is an unstable phenomenon driven by energy, it is of great use to reveal the disturbing impact of depressurizing boreholes on the roadway stability from the angle of energy dissipation. This is much more consistent with the failure nature of rock mass. Hence, an integrated method of laboratory test, numerical simulation, and theoretical analysis was used to study the disturbing effect of depressurizing boreholes on roadway energy dissipation. The equations of elastic energy and dissipated energy of rock cell grid were derived based on the energy principle and finite-difference algorithm, which was implemented into FLAC^{3D} software by the FISH language. The numerical stress-strain and dissipated energy-strain curves of rock samples were verified by experimentally obtained data, and the whole deformation path from roadway excavation to instability was back-analyzed by the dissipated energy evolution. Based upon the energy model, the ratio of borehole diameter D to row spacing R (D/R) was selected as the variable to analyze the influence of borehole parameters on the depressurizing effect. The varying D/R leads to three depressurizing states: insufficient depressurization, sufficient depressurization, and overdepressurization. Increasing D/R will make the roadway transfer from insufficient depressurization to sufficient depressurization and finally to overdepressurization. The sufficient depressurizing state could be realized by adjusting the borehole D/R value, which is of great use to the roadway control. The D/R values of 1 : 6 to 1 : 2 were proposed for the test roadway, and $D/R = 1 : 6$ was applied in the field test, which achieved a well roadway control effect.

1. Introduction

In China, lots of coal mines have successively shifted into the deep mining with the increase of mining intensity [1]. Compared to the shallow coal seam mining, the mechanical behaviors of coal/rock masses at deep depth changes fundamentally. As a result, the roadway is prone to nonlinear large deformation, which leads to the rock burst, coal and gas outburst, or other dynamic disasters in serious cases [2–4]. The instability events still occur in coal mines even when measures were implemented in the field, including increasing support strength and repairing large deformed roadway more times [5–8]. Hence, how to effectively control the deep roadway stability is still a major issue that affects the safety of recovering the deep coal resources [9].

Scholars pointed out that the stress, lithology, and support are the three main factors affecting the stability of deep roadways [10–13]. Previous studies on roadway control mainly focused on the latter two factors, lithology and support. Measures which focused on these two factors were applied, such as excavating the roadway in the rocks with high strength [14] or using the high-strength support to

control roadway deformation [15]. However, roadway failure that still emerges as the high stress is ignored [16]. The stress transfer technology, later also referred to as depressurization, was invented to reduce the impact of high stress [17]. This approach transfers the high stress around the roadway surface into the deeper stable rock masses by artificially weakening the bearing capacity of surface rocks [18]. The stress transfer technology has been widely applied in roadways subject to complex conditions, such as deep roadways, dynamic roadways, and soft rock roadways. Field tests showed that the stress transfer technology could make the roadway more stable than other control methods [19].

In China, stress transfer (depressurization) technology is classified into two categories according to its constructing locations, including depressurizing outside the roadway (DOR) and depressurizing inside the roadway (DIR) [20]. The frequently-used DOR technologies, such as tunneling the depressurizing roadway and mining of the depressurizing coal seam, produce a more favorable depressurizing effect than DIR (e.g., drilling boreholes [21], cutting trenches [22], and blasting for loosening [23]). However, an additional roadway or advancing face needs to be developed when using DOR technology, which is faced with issues of large amount of works and high costs. In fact, the DIR has been used more widely than DOR [24]. The depressurizing borehole belongs to the frequently used DIR technology. Compared to other depressurizing technologies, it has two advantages except for the high-stress transfer [25–29]: (1) boreholes could provide a compensation space for the deformation of rock masses, which decreases the roadway radial displacement. (2) Borehole drilling can be performed via mechanized operations, which is more safe and cost-effective. Hence, many existing literatures have presented studies on depressurizing boreholes. For example, Gao et al. used three-dimensional cables and depressurizing boreholes to control the roadway stability for the soft and thick coal seam [30]. Liu et al. controlled the large deformation of deep roadway using the depressurizing boreholes [31]. Wang et al. developed a composite technology, including depressurizing boreholes and bolt-grouting support, to control the high-stress roadway, and achieved a great success in field test [32].

The depressurizing boreholes have been widely used in the field, but inevitably, it has limitations. Most of the existing studies are focused on the stress transfer, and they lack the analysis of deformation control and roadway stability [20]. These make it difficult to quantitatively evaluate the depressurizing degree of roadway and to help design the borehole parameters. The borehole diameter D and row spacing R were considered as the key variables affecting depressurizing degree. These two parameters affect each other, and the interaction between these two parameters needs to be considered to achieve the optimum borehole parameters. However, the interaction was frequently ignored during the determination of the borehole parameters [33].

In the authors' previous studies, we tried to evaluate the depressurizing degree from the angle of stress transfer and deformation control of the roadway. The main problem is that it is difficult to evaluate the stress transfer effect of the depressurizing boreholes [32, 33]. In addition, using two indexes (stress and deformation) to evaluate the depressurizing effect complicated the analytical process. Given that the energy evolution occurs during the roadway deformation, energy dissipation in the surrounding rocks will be enhanced by drilling depressurizing boreholes [34, 35]. Analyzing the depressurizing degree from the view of energy dissipation can simplify the analytical process, as it can consider the stress and deformation at the same time. In this study, the energy equations were implemented into FLAC^{3D} software, and the disturbing effect of depressurizing boreholes on roadway stability was discussed from the view of energy dissipation. The influence of borehole diameter and row spacing on the damage degree of the surrounding rocks was revealed, which can provide guidance for the design of depressurizing borehole parameters.

2. Development and Application of Energy Models

2.1. Development of the Energy Model in FLAC^{3D}. The stress redistribution will occur after roadway excavation. Assuming that the process occurs in a closed system without the outside energy exchange, part of the energy generated by the stress redistribution is stored in the surrounding rocks as elastic energy, while the other part is consumed along the roadway deformation. The higher the damage degree of rock masses becomes, the lesser the elastic energy remains, and the more the energy is dissipated [36, 37]. Hence, based on the energy conservation and FLAC^{3D} difference operation principle, the expressions of elastic energy and dissipated energy can be derived according to the stress-strain relationship of rock elements. The specific calculation steps were given in the following.

In FLAC^{3D}, if the stress σ_i^I at time t and total strain increment $\Delta\varepsilon_i$ at time Δt were given, the new stress σ_i^N of cell grids could be solved at time $t + \Delta t$ [38]. Assuming that the Δt corresponds to the time-steps m, the formula of the total energy increment is described as

$$\Delta W_z = \sigma_i \Delta\varepsilon_i \quad (i = 1, 2, 3), \tag{1}$$

where i represents the three directions of the space rectangular coordinate system, and σ_i is the element stress corresponding to time-steps m, which can be represented by the average stress $\bar{\sigma}_i$ of the cell grids before and after the numerical operation. Then, the formula can be expressed as

$$\bar{\sigma}_i = \frac{1}{2}\left(\sigma_i^I + \sigma_i^N\right) \quad (i = 1, 2, 3). \tag{2}$$

Note that the m value is smaller and the element energy calculated by formula (1) is more accurate. By comparing numerical calculation with theoretical calculation, when $m \leq 20$, the error of them is controlled within 5%, so the value of m in the study is 20. Supposing that the time-step m is a computing loop, the total input energy of the cell grids after n loops can be written as

$$W_z = \sum_0^n \Delta W_z. \quad (3)$$

If the attenuation of postpeak elastic modulus E was ignored, the elastic energy accumulated in the cell grids can be calculated by the following formula:

$$W_e = \frac{1}{2}\sum_0^n \frac{{\sigma_i}^2}{E} \quad (i = 1, 2, 3). \quad (4)$$

Subtracting formula (4) from formula (3), the dissipative energy formula of cell grids can be obtained as

$$W_d = \sum_0^n \Delta W_z - \frac{1}{2}\sum_0^n \frac{{\sigma_i}^2}{E} \quad (i = 1, 2, 3). \quad (5)$$

The three variables, ${\sigma_i}^I$, ${\sigma_i}^N$, and $\Delta\varepsilon_i$, can be captured by the indicator functions in FLAC^{3D} [38]. Hence, equations (1) to (5) can be easily realized in FLAC^{3D} by the inbuilt FISH language. The implementing processes are given in Figure 1. Firstly, the numerical model is established and the rock mass parameters are determined. The end-step Q and the loop-step m can be defined, and the initial stress ${\sigma_i}^I$ of each cell grid is captured before the operation. Then, the operation is started and the new stress ${\sigma_i}^N$ and strain increment $\Delta\varepsilon_i$ are captured again after time-steps m. After that, the elastic energy and dissipated energy are calculated by equations (4) and (5). The whole loop will continue until the end-steps Q. Finally, the energy nephograms of the cell grids are achieved.

2.2. Application of the Energy Model

2.2.1. Engineering Background. The coal transporting main roadway (see the blue thick line in Figure 2) in the Sanhejian coal mine of Xuzhou Mine Group was selected as the engineering background. The roadway is connected to the -700 m west main roadway in the east and adjacent to the F1-1 fault in the south, where the north side is the gobs. The buried depth of the test roadway is about 800 m, and the total length is 1442 m. The main apparent lithology along the roadway is fine sandstone and siltstone (see the borehole columnar section at the lower-right corner of Figure 2). Fine sandstone accounts for about 75% of the total roadway length. According to the in situ stress test, the maximum principal stress along the roadway is gravity stress, and the horizontal stress is about 80% of the gravity stress [39]. The roadway was developed in the form of a straight wall with a semicircular arch roof with a section size (width × height) of 5.0 m × 4.0 m. Rock bolts with row spacing of 800 mm × 800 mm were adopted after excavation.

The location at 400 m away from the roadway opening (see the red solid point in Figure 2) was selected for the field monitoring, because this location was outside of the influence of the fault and mining activities. The roadway deformation at the measure point is shown in the top-left pictures in Figure 2. The large deformation mainly occurred in the roadway floor and two ribs, where the maximum convergences exceeded 1000 mm. The transportation work of the roadway has been interrupted by the large deformation, which requires renovation.

2.2.2. Simulation of the Rock Mechanics Test Based on the Energy Model. To calibrate the numerical simulation results, the experimental tests subject to 6 different confining stresses of 0 MPa, 5 MPa, 10 MPa, 15 MPa, 20 MPa, and 25 MPa were carried out in the laboratory. The test results were detailed in Ref. 40. The objective of this section is to verify the energy model using the experimentally obtained results. The size of numerical rock samples was in the diameter of 50 mm and in the height of 100 mm, which is the same as the laboratory test (see Figure 3(a)). The rock parameters obtained from the laboratory test were implemented into the model [40]. The bottom boundary of the model was fixed, the confining pressure was applied to the side boundary, and the axial displacement was applied to the upper boundary to simulate the loading. After that, the energy codes given in Section 2.1 were called to perform the calculation.

To simplify the analysis, the test with confining pressure of 5 MPa was selected and used here [40]. It can be seen from Figure 3(b) that the power generated by the loading stress was stored inside rock samples as elastic energy when the rock samples were in the prepeak stage, and at the same time, the dissipated energy remained at a very small value (almost zero). Once the rock samples entered the postpeak phase, the dissipated energy increased dramatically until it reached the residual stage where the dissipated energy gradually leveled off. The stress-strain and dissipated energy-strain curves obtained from the numerical simulation were in the high agreement with the experimental results. Since the elastic modulus E is assumed to be constant when calculating energy, there is no energy attenuation before the peak. The focus of this paper is on the description of postpeak failure. Therefore, this hypothesis has no influence on postpeak failure of rock mass. However, it should be noted that if the prepeak compaction and plastic deformation must be analyzed, the effect of elastic modulus E on prepeak energy change needs further consideration.

2.2.3. Simulation of Roadway Deformation Based on the Energy Model. A roadway simulation was also carried out to verify the applicability of the energy model in the analysis of engineering problems. The model size was 60 m in length (X axis), 40 m in width (Y axis), and 60 m in height (Z axis). The stress boundaries, roadway section size, and supporting parameters were consistent with the field case. The strain-softening Mohr-Coulomb criterion was used in the model. It should be noted that the rock mass parameters need to be verified before the simulation. For the sake of simplification, the fine sandstone section exposed in the test roadway is taken as the research object, because this section accounts for about 75% of the total roadway length. The strength properties of the rock samples were converted to those of the rock masses using RocLab software, which were assigned to the model as the initial parameters. Afterwards, the optimal parameters of rock masses were determined by

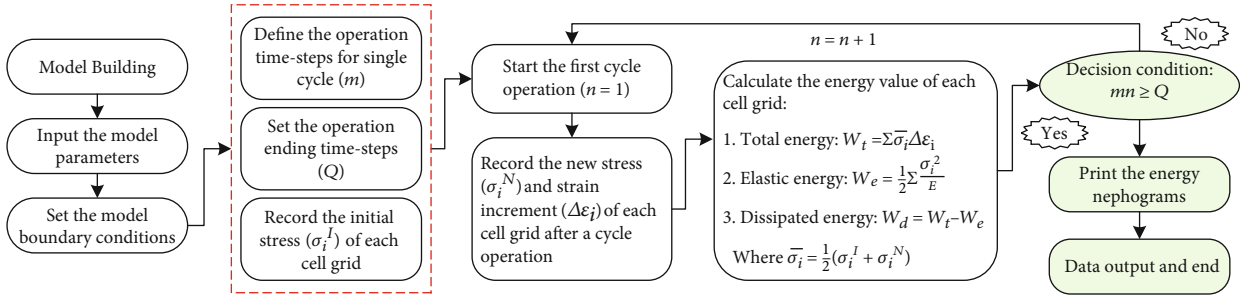

Figure 1: Flow chart of cell grid energy calculation in FLAC^{3D}.

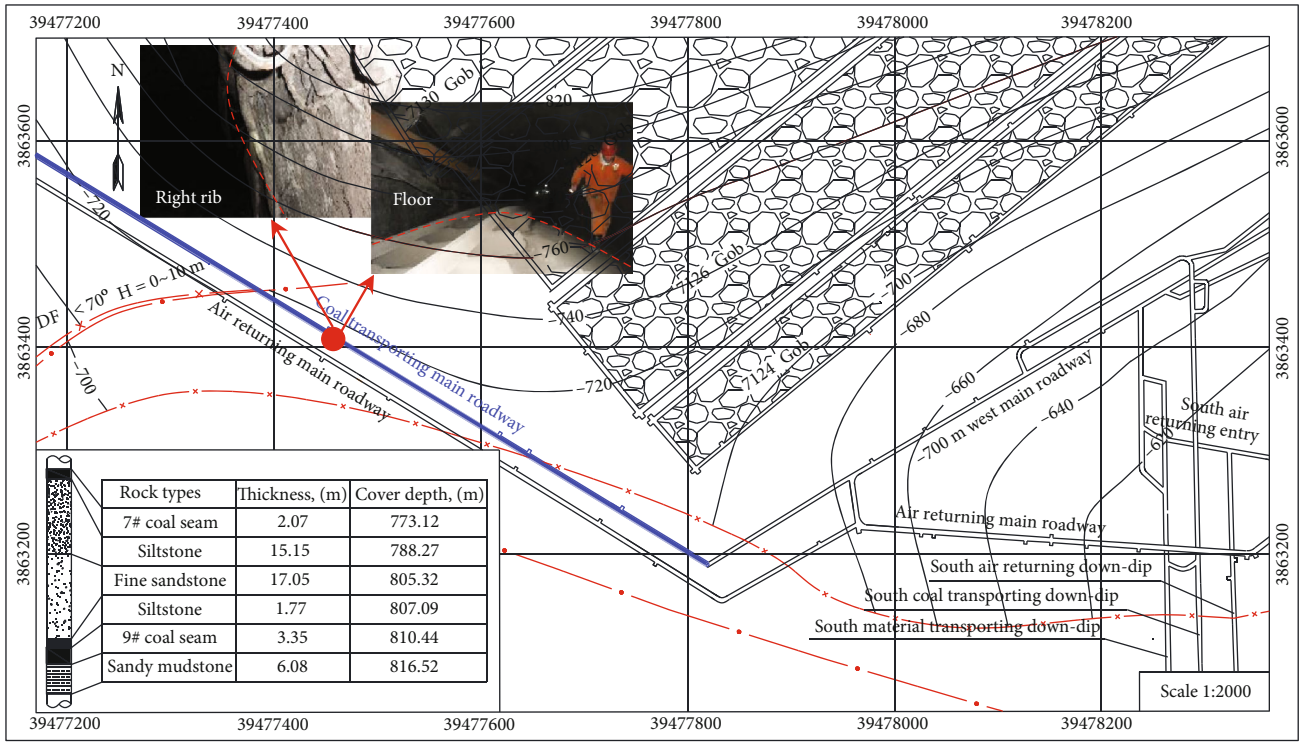

Figure 2: Layout of the test site in the Sanhejian coal mine. The lower-left corner gives the borehole columnar section of the test roadway. The thick blue line represents the test roadway position. The red solid point is the location where these roadway deformation photos were taken.

comparing with roadway failure ranges in the field. The calibrated parameters of the rock masses are given in Table 1.

In Figures 4(a) and 4(b), the dissipated energy density (DED) and the distribution cloud of the plastic zone are given, respectively. The vertical stress distribution of roadway ribs is shown in the curve of Figure 4(b). By comparing Figure 4(a) with Figure 4(b), the stress peak of the roadway wall is 7.5 m away from the center point of the roadway, and the expansion range of roadway dissipated energy is basically the same as the plastic zone. The roadway deformation path and main failure positions could be revealed by the dissipated energy evolution; however, it cannot be realized with the plastic zone analysis.

Analysis from Figure 4, the maximum principal stress of roadway is the gravity stress, and the stress concentration after excavation will be generated in the two ribs. The concentrated stresses cause the rib large deformation; meanwhile, they will intensify the floor extrusion flow when the stress was transferred to the floor [41]. In other words, the elastic energy accumulations caused by stress redistributions in roadway ribs provided a sustained power for the ribs and floor deformation.

For the test roadway, drilling the rib depressurizing boreholes is the effective approach to control its large deformation, because the depressurizing boreholes will absorb the rib deformation and also prevent the high stress from transferring to the roadway floor. However, attention should be paid to the depressurizing degree of roadway as a reasonable depressurizing degree plays a vital role in the control effect. Considering that the borehole diameter D and row spacing R are the main factors affecting the roadway depressurizing degree, in the following sections, the energy

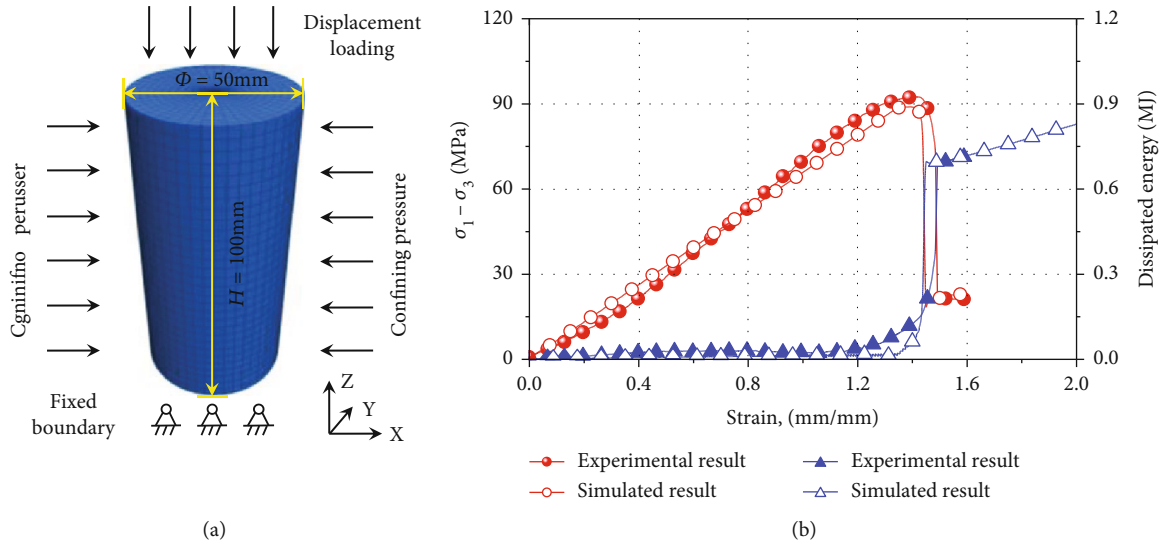

Figure 3: Comparisons between the numerical simulation and laboratory test. (a) Represents the numerical model of rock samples. (b) Gives the stress-strain and dissipated energy-strain curves obtained from numerical modeling and laboratory test, respectively.

Table 1: Calibrated parameters of the rock masses.

Prepeak	Elasticity modulus E (GPa)	Poisson ratio μ	Cohesion c (MPa)	Internal friction angle φ (°)	Tensile strength σ_t (MPa)
	2.09	0.26	3.61	30.36	0.4
Postpeak	Plastic strain ε^{ps}	0.01	0.02	0.5	1
	Cohesion c (MPa)	2.61	1.60	0.32	0.32
	Internal friction angle φ (°)	30.72	24.64	23.14	23.14

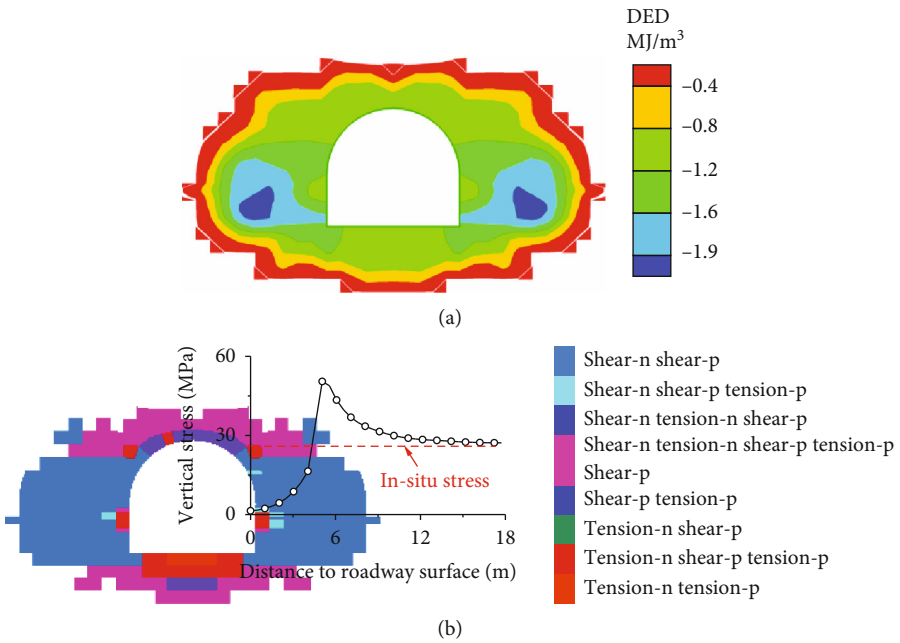

Figure 4: Numerical simulation results. (a) and (b) represent the evolvements of roadway dissipated-energy density (DED) and plastic zone, respectively. The curve in (c) is the vertical stress distribution of the roadway ribs.

model will be used to discuss the influence of D and R on the roadway stability.

3. Impact of Depressurizing Boreholes on Roadway Energy Dissipation

3.1. Model Setup of the Depressurizing Boreholes. Drilling depressurizing boreholes aims to release the elastic energy inside the roadway ribs. To facilitate the boreholes excavating, the rib meshes of the numerical model established in Section 2.2.3 were modified by HyperMesh software. In the modified model (see Figure 5), the boreholes were placed in the Y direction with a minimum row spacing (R) of 0.6 m, while each row (Z direction) contains up to four horizontal boreholes with 0.6 m interspacing (I). Four possible values, 100 mm, 200 mm, 300 mm, and 400 mm (see Figure 5(a)), were considered for the borehole diameters (D). These pretreating can realize the borehole excavation under the different schemes of R, I, and D. Note that the interspacing was fixed as 1.2 m due to the fact that it is difficult to drill multiple rows of boreholes in the circumferential direction. The parameters and boundary conditions of the rock masses were similar to those of the above model in Section 2.2.3.

3.2. Numerical Simulation Schemes. Ref. 32 pointed out that the borehole length affected the movement distance of the peak-stress zone, and it should be determined to penetrate the stress concentration area. In addition, a maximum of two rows of borehole generally could be constructed in the roof, rib, or floor, because of the limitation of roadway size and construction equipment [33]. Hence, the borehole diameter D and row spacing R were chosen as variables to carry out this study, while the borehole interspacing I was fixed as 1.2 m [33] (see Figure 5(a)), and the borehole length was determined as 9 m because the stress concentration area distributed in the range of 4 to 9 m from the roadway surface (see Figure 4(b)). Considering the correlation between borehole diameter D and row spacing R, the D/R ratio was used to design the simulation schemes as shown in Table 2. By the numerical simulation, borehole excavation with different D/R was carried out at the same time with roadway excavation. After excavation of roadway and boreholes, time-step control numerical simulation is used.

3.3. Simulation Results of the DED Distributions with Different D/R. Figures 6(a)–6(f) show the dissipated energy density (DED) distributions of roadway under different D/R ratios. As shown in Figure 6, when $D/R = 2:3$ and $1:2$, the peak values of DED distribute at the boundary of depressurizing zone (borehole excavation area), and DED has a larger magnitude. Once the D/R is less than $1:2$, the DED peaks locate in the middle of neighboring boreholes. As the D/R decreases, the interplay between the neighboring boreholes decreases and the DED profile eventually changes from the state of "single peak value" to the "double peak values," and the peak value of the DED gradually decays. When $D/R < 1:6$, the influence range of neighboring boreholes cannot superimpose, and the DED distribution generated by each borehole exists in an isolated state. Those indicate that a smaller D/R could lead to smaller energy dissipation and less depressurizing influence.

The DED values extracted from the central location of neighboring boreholes with different D/R ratios are shown in Figure 7. For the roadway without boreholes (see Figure 4(a) and blue curve in Figure 7), the evolution range of DED reaches 5 m from the roadway surface with the peak value of 2.5 MJ/m^3. When $D/R = 1:10$ and $1:8$, the depressurizing boreholes have a slight influence on the roadway energy dissipation. Once the $D/R > 1:8$, the DED extended range increases sharply. For instance, when $D/R = 1:6$, the DED extended range increases to 9 m. Afterwards, the DED range gradually levels off with the further increase of the D/R ratio, as the designed borehole length of 9 m limits the roadway depressurizing range.

Increasing the D/R ratio would dramatically affect the DED within the effective depressurizing area (9 m from the roadway surface). As the D/R increases from $1:6$ to $2:3$, the DED peak value increases initially and then decreases afterwards. The peak values of DED for $D/R = 1:6$, $1:4$, $1:2$, and $2:3$ are 4.01 MJ/m^3, 8.43 MJ/m^3, 9.22 MJ/m^3, and 8.30 MJ/m^3, respectively. The larger the D/R is, the closer the DED peak is to the roadway surface, which indicates that a higher depressurizing degree will occur. Once D/R increases to certain critical values (e.g., $2:3$), the elastic energy stored in the surrounding rock would reduce significantly because it is subject to serious damage, which will result in the attenuation of DED values. Those cases are extremely dangerous for roadway control, as it is difficult to maintain the stability of fractured rock masses once they lost the bearing capacity.

In the above analysis (as shown in Figure 7), the DED distributions in the direction paralleled to borehole drilling (X axis) were grasped. In the following, discussions on DED distributions between neighboring boreholes along the roadway excavation (Y axis) will be carried out. As shown in Figure 4(b), the peak stress is located at 5 m from the roadway surface, approximately located in the middle of borehole length. The characteristic stress position (peak stress, $X = 7.5$ m in Figure 5) was selected as the study object, and the DED data between neighboring boreholes is shown in Figure 8.

As shown in Figure 8, when $D/R = 2:3$, the DED distribution exhibits approximately a straight line, which means a higher energy dissipation with the magnitude of 7.5 MJ/m^3. When D/R decreases to $1:2$, the DED distributing curve has a "single peak value" of about 8.85 MJ/m^3. Once $D/R < 1:2$, the DED curves change from "single peak value" to "double peak values" and distribute symmetrically along the neighboring borehole center. In addition, the DED peak value decreases with the decreasing D/R, implying the attenuations of the depressurizing degree. Note that when $D/R = 1:8$ and $1:10$, the DED curves have a "zero value section," and its length increases with the decreasing D/R. The "zero value section" indicates the presence of the undisturbed region between the neighboring boreholes due to the lack of interplay.

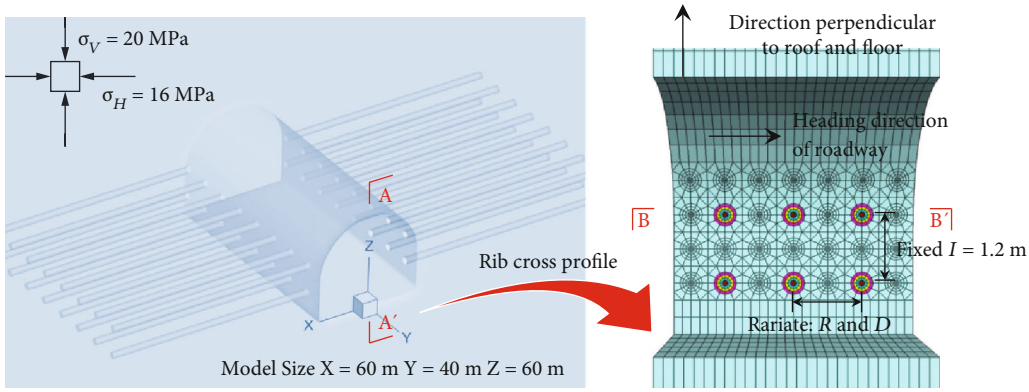

Figure 5: Numerical model containing depressurizing boreholes in FLAC^{3D}. (a) Illustrates the cross section of one rib along the longitude direction of roadway. The distance between the neighboring boreholes in the heading direction of roadway was defined as row spacing R, while that in the direction perpendicular to the roof and floor was termed as interspacing I. The interspacing I was fixed as 1.2 m, while D and R were chosen as the variables in this study. D and R will be constructed according to the design schemes.

Table 2: Simulation schemes for the depressurizing boreholes.

Constants	Orientation Horizontal boreholes drilled in ribs		Length 9 m		Interspacing 1.2 m	
Simulation schemes	I	II	III	IV	V	VI
D/R	2 : 3	1 : 2	1 : 4	1 : 6	1 : 8	1 : 10
Diameter	400 mm	300 mm	300 mm	300 mm	300 mm	300 mm
Row spacing	600 mm	600 mm	1200 mm	1800 mm	2400 mm	3600 mm

Note that the simulation results without boreholes were regarded as a reference for comparison.

Based on the characteristics of the DED distributing curves in Figures 7 and 8, the three depressurizing states could be summarized: (1) Insufficient depressurization. When $D/R < 1 : 6$, the depressurizing boreholes partially disturbed the roadway surrounding rock, which causes the existence of "zero value section" of DED curves. (2) Sufficient depressurization. When $1 : 6 \le D/R \le 1 : 2$, the influence area of boreholes could cover the entire depressurizing range, and the DED maintains a higher magnitude. (3) Overdepressurization. When $D/R > 1 : 2$, the DED in roadway ribs is almost a straight line, and its peak value inversely decreases, which is harmful to the roadway control.

3.4. Simulation Verifications for the Depressurizing Degree Classification. In Section 3.3, the depressurizing states were classified into three categories: insufficient depressurization, sufficient depressurization, and overdepressurization based on the characteristics of DED curves. The rationality of the corresponding D/R to the three depressurizing states will be justified from the angle of using relief borehole drilling to control the roadway deformation. Figures 9 and 10 give the displacement curves of ribs and floor under various D/R ratios, respectively. For the sake of simplification, the roof control by boreholes was not considered because the large deformation of roadway primarily occurs in the ribs and floor.

As shown in Figure 9, prior to depressurizing borehole drilling, the rib convergences mainly occur in the range of 0 to 5 m from the roadway surface. For instance, the rib convergences are 305 mm, 199 mm, and 3 mm at the locations of 0 m, 1.5 m, and 6 m distancing from roadway surface (see the first columns of Figures 9(a)–9(c)), respectively. The rib convergence within the scope of 5 m significantly decreases after the borehole drilling, but its amplitude reduction has the following differences: (1) when $1 : 6 \le D/R \le 1 : 2$, the rib convergence in the 5 m scope decreases with the increase of D/R, while the deformation beyond 5 m away from roadway surface slightly increases due to the borehole drilling. (2) When $D/R < 1 : 6$, the rib surface convergence has almost no differences compared to that without boreholes, because the low borehole density is insufficient to absorb the deformation of the surrounding rock mass. (3) When $D/R = 2 : 3$, the rib convergence becomes larger than that of $D/R = 1 : 2$, which is caused by the overdepressurization.

As shown in Figure 10, the depressurizing borehole drilling could effectively control the floor deformation. For roadways without boreholes, the convergences that occurred at the floor surface and 3 m below are 288 mm and 86 mm, respectively. For roadways with boreholes, the convergence at the floor surface remains in the range of 150 mm to 193 mm, and it decreases with the increasing D/R. On the contrary, the increase of D/R leads to the slightly larger deformation of rock mass at 3 m below the floor surface. The essence of drilling rib boreholes to control floor heave is that the boreholes cut off the transferring paths of elastic energy stored in

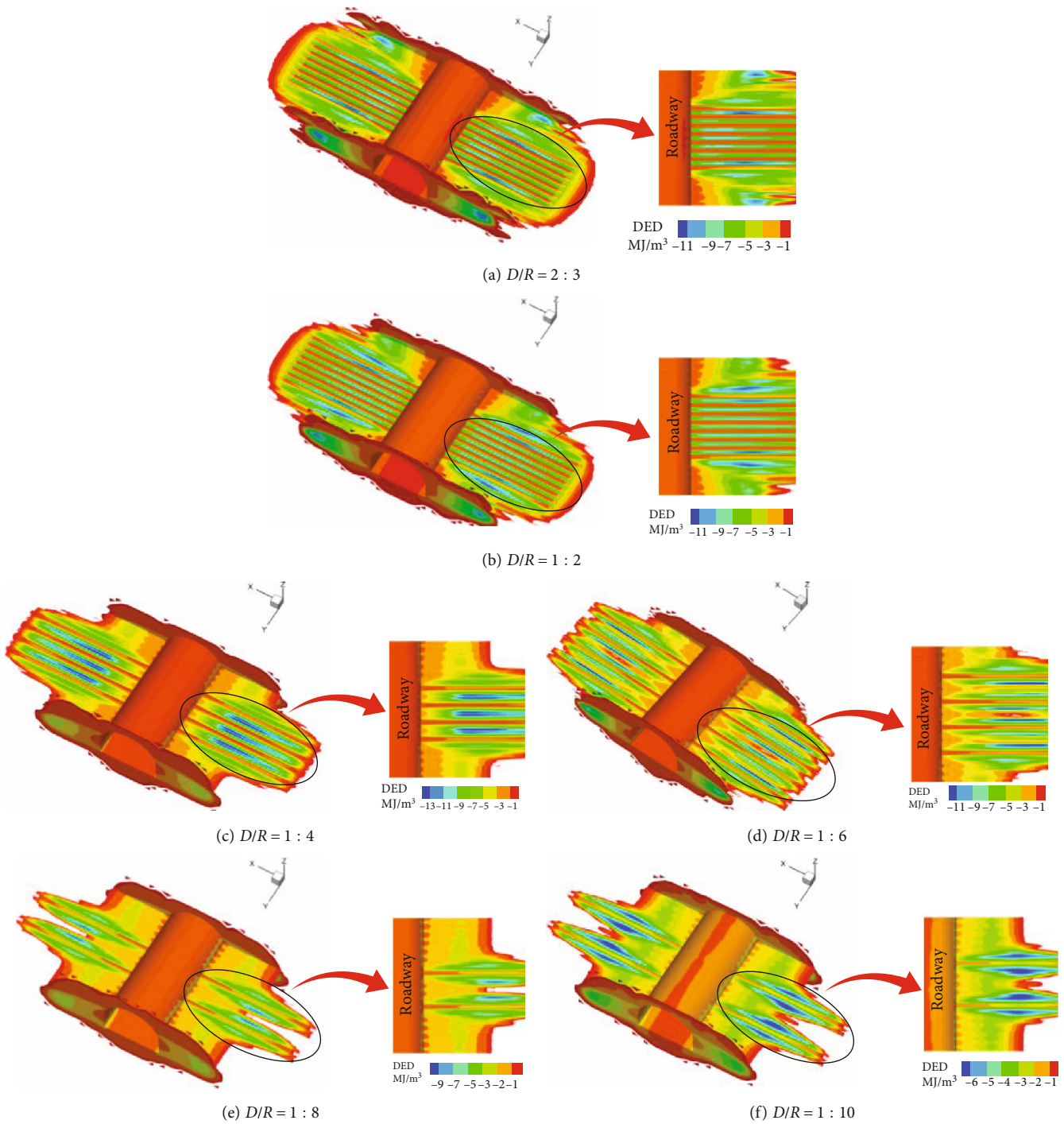

Figure 6: Dissipated energy density (DED) distributions of roadway under different borehole D/R ratios. Note that the data were obtained from the profile as shown in B-B′ of Figure 5(a).

the ribs. The floor extrusion flow can be alleviated after the floor rock mass lost the power source, which results in the floor deforming continuously.

Based on the above analysis, the insufficient depressurization and overdepressurization could not improve the roadway stability. The former has a limited impact on the roadway control, while the latter could result in larger deformation. The roadway could be effectively controlled only when the sufficient depressurization is used. The depressurizing degree classification by the DED distribution is justified from the view of the roadway deformation control. For the test roadway, the D/R which can be used to control its large deformation could be defined as $1 : 6 \leq D/R \leq 1 : 2$.

3.5. Verifications of the Field Application. For the test roadway, the accumulations of elastic energy in both ribs were the main reason causing the roadway large deformation, and the depressurizing borehole drilling aims to increase

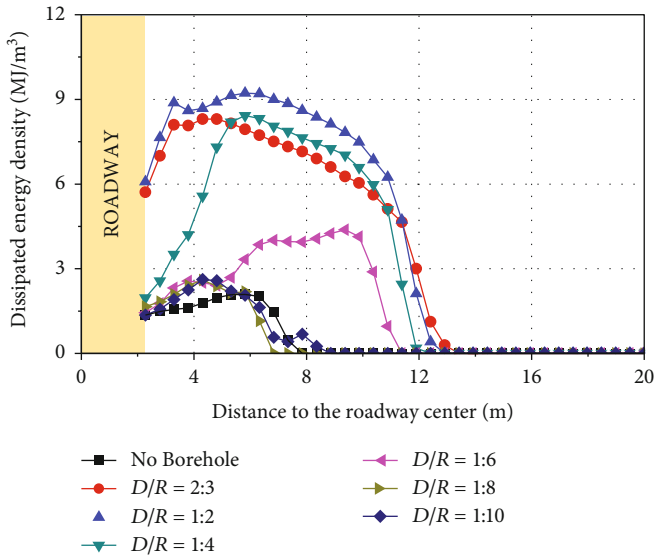

FIGURE 7: DED distributing curves between the neighboring boreholes in X direction under different D/R ratios. The data were extracted from the B-B′ section in Figure 5(a).

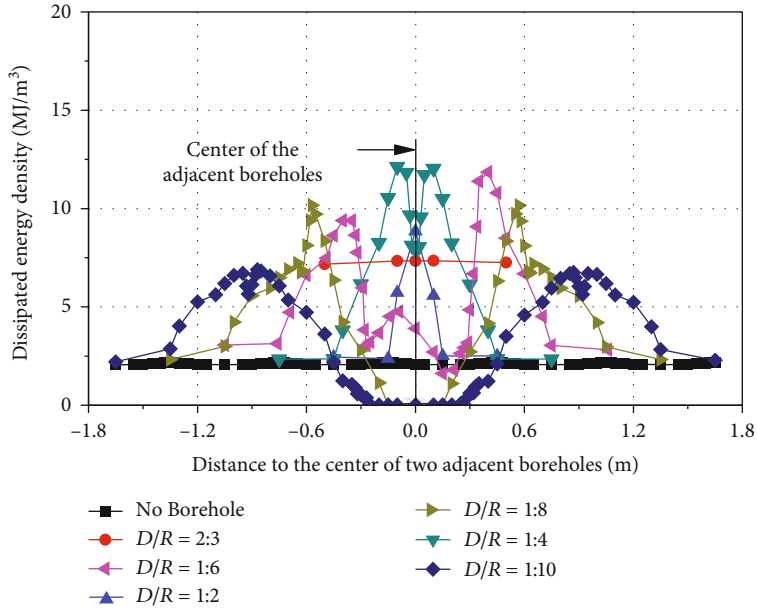

FIGURE 8: DED distributing curves between the neighboring boreholes at $X = 7.5$ m in Y direction under different D/R ratios. The data were extracted from the B-B′ section in Figure 5(a). The "0" point indicates the midpoint of the circle center line of the adjacent boreholes.

the energy dissipation in the ribs. The reasonable D/R values were identified as $1:6 \le D/R \le 1:2$. In the Sanhejian coal mine, the available drilling rig could perform the maximum borehole diameter of 150 mm. Hence, the borehole row spacing was designed as 900 mm by the relation of borehole diameter and row spacing corresponding to the sufficient depressurization (150 mm × 6 = 900 mm). Two boreholes were drilled in each row of roadway ribs with the interspace of 900 mm and length of 9 m. Figure 11 shows the comparison of the roadway deformation before and after depressurization. The deformation that occurred in roadway ribs and floor after depressurization was only 40% of that without boreholes.

Note that the upper limit of the D/R value (1:6) corresponding to sufficient depressurization was used to determine the borehole row spacing. The purpose of doing this is to prevent the overdepressurization. If the roadway is in insufficient depressurization, extra boreholes could be conducted to increase the depressurizing degree. However, once the roadway enters into the overdepressurization, the excessive deformation will make it extremely difficult to maintain the stability of roadway.

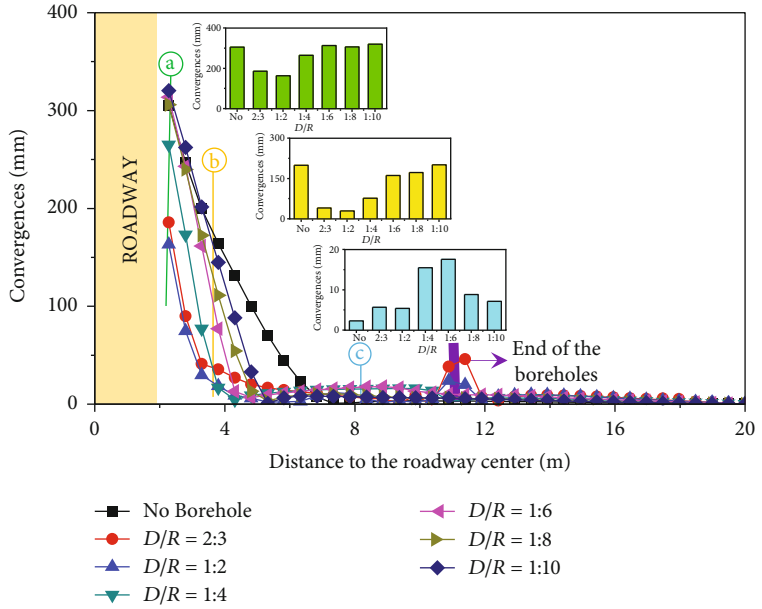

Figure 9: Rib convergence curves under the different borehole D/R ratios. (a–c) Represents the rib convergence at the locations of 0 m, 1.5 m, and 6 m distancing from the rib surface, respectively.

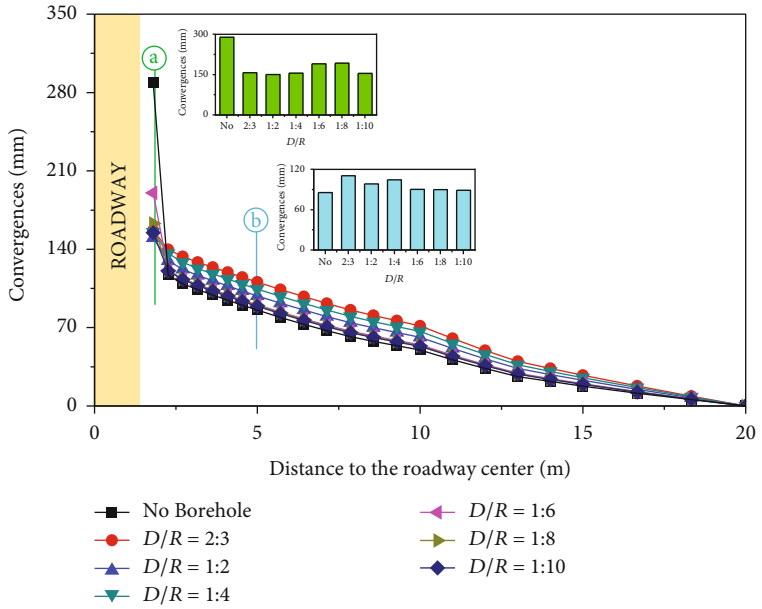

Figure 10: Floor convergence curves under the different borehole D/R ratios. (a) and (b) give the rib convergence that occurred in the locations of 0 m and 3 m from the floor surface, respectively.

3.6. Discussions. The energy dissipation of roadway could be adjusted by changing the diameter and row spacing of depressurizing boreholes. The borehole diameter should be determined prior to the row spacing, because its value is controlled by the drilling rig power. Once the diameter is determined, the row spacing of boreholes can be obtained based upon the D/R ratio. Increasing the D/R, the depressurizing state of roadway will be transferred from insufficient depressurization to sufficient depressurization and finally to overdepressurization. The ideal depressurizing effect can be achieved only when a reasonable D/R value is selected.

In this study, only the row-by-row pattern of the depressurizing boreholes is considered in the present study. Other patterns of the boreholes, for example, staggered or triangular layouts, may also be employed to reduce roadway convergence. The future study with different borehole D/R and layouts will be conducted in order to reach the maximum technical and economic benefits.

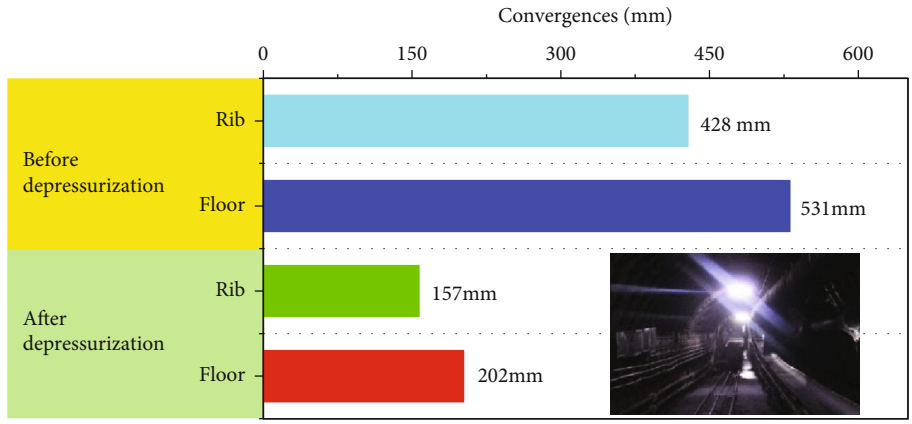

Figure 11: Comparison of the roadway deformation before and after depressurization. The photograph at the lower-right corner shows the roadway maintenance with drilling depressurizing boreholes.

In addition, the parameters of depressurizing boreholes are determined by dissipative energy distribution of rock mass and are verified by field test and numerical simulation which better verified the accuracy of borehole parameters. When borehole parameters are designed, the displacement check can be simplified and only from the energy evolution curve of adjacent boreholes, which saves a great deal of time than using stress and displacement bivariate analysis. Compared with the previous research work (Ref. 32), the borehole parameters determined by dissipative energy are more accurate than those determined by stress.

4. Conclusions

This study makes an attempt to reveal the impact of relief hole drilling on the roadway stability from the view of energy dissipation, which provides a basis for the determination of borehole parameters. The conclusions obtained are shown in the following.

(1) Based on the energy principle and finite-difference algorithm, the formulas of elastic energy and dissipated energy of rock cell grid were derived and were implemented in the FLAC^{3D} software by FISH language. The main roadway in the Sanhejian coal mine was chosen as the engineering background. The numerical model was calibrated by the stress-strain and dissipated energy-strain curves of rock samples. Additionally, the deformation paths from roadway excavation to instability were modeled using the dissipated energy evolution

(2) The ratio of borehole diameter to row spacing (D/R) was selected as the variable to study the influence of borehole parameters on the energy dissipation and stability of roadway. It was concluded that there are three depressurizing states, insufficient depressurization, sufficient depressurization, and overdepressurization, due to the different D/R. By increasing the D/R, the depressurizing state will be transferred from insufficient depressurization to sufficient depressurization and finally to overdepressurization. If the roadway is in the insufficient depressurization, a depressurizing blind section where DED equals to zero appears between the neighboring boreholes. When the roadway is in the overdepressurization state, the roadway deformation will increase, which is harmful for the roadway maintenance. A reasonable D/R plays an important role in controlling the large deformation of deep roadway

(3) The D/R ratios of 1 : 6 to 1 : 2 are suggested for the test roadway, and the D/R of 1 : 6 was applied in the field application. The monitoring results showed that the deformation occurred in roadway ribs and floor after depressurization was only 40% of that without boreholes. The depressurizing borehole drilling is capable of controlling the stability of roadway

Data Availability

The data used to support the findings of this study are available from the corresponding author upon request.

Conflicts of Interest

The authors declare that they have no known competing financial interests or personal relationships that could have appeared to influence the work reported in this paper.

Acknowledgments

The authors are grateful for the financial support from the National Natural Science Foundation of China (contract nos. 51704098 and 52174074), the Science Foundation for Outstanding Youth of Henan Province (contract no. 222300420048), and the Project Supported by the Distinguished Young Scholars Foundation of Henan Polytechnic University (contract no. J2021-4).

References

[1] W. J. Yu, W. J. Wang, X. Y. Chen, and S. H. Du, "Field investigations of high stress soft surrounding rocks and deformation control," *Journal of Rock Mechanics and Geotechnical Engineering*, vol. 7, no. 4, pp. 421–433, 2015.

[2] X. B. Li, C. J. Li, W. Z. Cao, and M. Tao, "Dynamic stress concentration and energy evolution of deep-buried tunnels under blasting loads," *International Journal of Rock Mechanics and Mining Sciences. vol.*, vol. 104, pp. 131–146, 2018.

[3] Z. L. Li, X. Q. He, L. M. Dou, D. Z. Song, and G. F. Wang, "Numerical investigation of load shedding and rockburst reduction effects of top-coal caving mining in thick coal seams," *International Journal of Rock Mechanics and Mining Sciences*, vol. 110, pp. 266–278, 2018.

[4] W. Shen, G. Shi, Y. Wang, J. Bai, R. Zhang, and X. Wang, "Tomography of the dynamic stress coefficient for stress wave prediction in sedimentary rock layer under the mining additional stress," *International Journal of Mining Science and Technology*, vol. 31, no. 4, pp. 653–663, 2021.

[5] Q. Li, R. Yang, J. Li, W. He, and Z. Wen, "Strength and cost analysis of new steel sets as roadway support project in coal mines," *Advances in Materials Science and Engineering*, vol. 2018, Article ID 3927843, 9 pages, 2018.

[6] S. W. Liu, D. Y. He, and M. X. Fu, "Experimental investigation of surrounding-rock anchoring synergistic component for bolt support in tunnels," *Tunnelling and Underground Space Technology*, vol. 104, article 103531, 2020.

[7] G. J. Wu, W. Z. Chen, S. P. Jia et al., "Deformation characteristics of a roadway in steeply inclined formations and its improved support," *International Journal of Rock Mechanics and Mining Sciences*, vol. 130, p. 104324, 2020.

[8] S. Q. Yang, M. Chen, H. W. Jing, K. F. Chen, and B. Meng, "A case study on large deformation failure mechanism of deep soft rock roadway in Xin'An coal mine, China," *Engineering Geology*, vol. 217, pp. 89–101, 2017.

[9] H. Wagner, "Deep mining: a rock engineering challenge," *Rock Mechanics and Rock Engineering*, vol. 52, no. 5, pp. 1417–1446, 2019.

[10] H. P. Kang, "Support technologies for deep and complex roadways in underground coal mines: a review," *International Journal of Coal Science & Technology*, vol. 1, no. 3, pp. 261–277, 2014.

[11] X. F. Guo, Z. Q. Zhao, X. Gao, X. Y. Wu, and N. J. Ma, "Analytical solutions for characteristic radii of circular roadway surrounding rock plastic zone and their application," *International Journal of Mining Science and Technology*, vol. 29, no. 2, pp. 263–272, 2019.

[12] K. P. Yu, F. Y. Ren, R. Puscasu, P. Lin, and Q. G. Meng, "Optimization of combined support in soft-rock roadway," *Tunnelling and Underground Space Technology*, vol. 103, p. 103502, 2020.

[13] J. Chen, P. Liu, L. Liu et al., "Anchorage performance of a modified cable anchor subjected to different joint opening conditions," *Construction and Building Materials*, vol. 336, p. 127558, 2022.

[14] H. P. Kang, J. Lin, and M. J. Fan, "Investigation on support pattern of a coal mine roadway within soft rocks — a case study," *International Journal of Coal Geology*, vol. 140, no. 15, pp. 31–40, 2015.

[15] R. Peng, X. R. Meng, G. M. Zhao, Z. H. Ouyang, and Y. M. Li, "Multi-echelon support method to limit asymmetry instability in different lithology roadways under high ground stress," *Tunnelling and Underground Space Technology*, vol. 108, p. 103681, 2021.

[16] J. Xie, M. Gao, R. Zhang, S. Li, Q. Tan, and Z. Qiu, "Lessons learnt from measurements of vertical pressure at a top coal mining face at Datong tashan mines, China," *Rock Mechanics and Rock Engineering*, vol. 49, no. 7, pp. 2977–2983, 2016.

[17] T. Goto, Y. Ishijima, S. Kinoshita, and N. Oda, "Effectiveness of relief boring in case of Akabira Colliery," *Journal of the Japan Institute of Metals and Materials*, vol. 93, no. 1068, pp. 75–81, 1977.

[18] F. Cheng, A. Chen, D. Wu, X. Tang, and S. Chunhui, "Numerical simulation of cracking failure and weakening law of roadway surrounding rock under high stress," *Shock and Vibration*, vol. 2021, Article ID 7236077, 11 pages, 2021.

[19] C. J. Hou, X. Y. Wang, and J. B. Bai, "Basic theory and technology study of stability control for surrounding rock in deep roadway way," *International Journal of Mining Science and Technology*, vol. 50, no. 1, pp. 1–12, 2021.

[20] C. Hou, "Ground control of roadway. Xuzhou, China (in Chinese)," 2013.

[21] S. Zhang, Y. Li, B. Shen, X. Sun, and L. Gao, "Effective evaluation of pressure relief drilling for reducing rock bursts and its application in underground coal mines," *International Journal of Rock Mechanics and Mining Sciences*, vol. 114, no. 2, pp. 7–16, 2019.

[22] D. Yang, X. Wang, Y. Wang, H. An, and Z. Lei, "Experiment and analysis of wedge cutting angle on cutting effect," *Advances in Civil Engineering*, vol. 2020, Article ID 5126790, 16 pages, 2020.

[23] A. G. Yardimci and M. Karakus, "A new protective destressing technique in underground hard coal mining," *International Journal of Rock Mechanics and Mining Sciences*, vol. 130, p. 104327, 2020.

[24] X. Cheng, G. M. Zhao, Y. M. Li, X. R. Meng, and Q. Y. Tu, "Key technologies and engineering practices for soft-rock protective seam mining," *International Journal of Mining Science and Technology*, vol. 30, no. 6, pp. 889–899, 2020.

[25] H. Liu, Y. Cheng, J. Song, Z. Shang, and L. Wang, "Pressure relief, gas drainage and deformation effects on an overlying coal seam induced by drilling an extra-thin protective coal seam," *International Journal of Mining Science and Technology*, vol. 19, no. 6, pp. 724–729, 2009.

[26] Z. L. Li, L. M. Dou, W. Cai, G. F. Wang, Y. L. Ding, and Y. Kong, "Roadway stagger layout for effective control of gob-side rock bursts in the longwall mining of a thick coal seam," *Rock Mechanics and Rock Engineering*, vol. 49, no. 2, pp. 621–629, 2016.

[27] J. Xie, J. Xu, and F. Wang, "Mining-induced stress distribution of the working face in a kilometer-deep coal mine-a case study in Tangshan coal mine," *Journal of Geophysics and Engineering*, vol. 15, no. 5, pp. 2060–2070, 2018.

[28] B. Lin, J. Zhang, C. Shen, Q. Zhang, and C. Sun, "Technology and application of pressure relief and permeability increase by jointly drilling and slotting coal," *International Journal of Mining Science and Technology*, vol. 22, no. 4, pp. 545–551, 2012.

[29] X. L. Yang, G. C. Wen, T. K. Lu et al., "Optimization and field application of CO_2 gas fracturing technique for enhancing CBM extraction," *Natural Resources Research*, vol. 29, no. 3, pp. 1875–1896, 2020.

[30] M. Gao, N. Zhang, C. Guo, and L. Dou, "Mechanics and practice of combined supporting technology of 3D anchor cable and unloading technology of wall of roadway," *Chinese Journal of Geotechnical Engineering*, vol. 27, no. 5, pp. 587–590, 2005.

[31] H. Liu, Y. He, J. Xu, and L. Han, "Numerical simulation and industrial test of boreholes destressing technology in deep coal tunnel," *Journal of China Coal Society*, vol. 32, no. 1, pp. 33–37, 2007, (in Chinese).

[32] M. Wang, D. J. Zheng, W. L. Shen, X. Y. Wang, and W. F. Li, "Depressurizing boreholes for mitigating large deformation of the main entry," *Energy Science & Engineering*, vol. 8, no. 4, pp. 1404–1417, 2020.

[33] M. Wang, X. Y. Wang, and T. Q. Xiao, "Borehole destressing mechanism and determination method of its key parameters in deep roadway," *Journal of China Coal Society*, vol. 42, no. 5, pp. 1138–1145, 2017.

[34] Z. P. Zhang, H. P. Xie, R. Zhang et al., "Deformation damage and energy evolution characteristics of coal at different depths," *Rock Mechanics and Rock Engineering*, vol. 52, no. 5, pp. 1491–1503, 2019.

[35] H. Xie, "Research framework and anticipated results of deep rock mechanics and mining theory," *Advanced Engineering Sciences*, vol. 49, pp. 1–16, 2017.

[36] Z. Zhang and F. Gao, "Confining pressure effect on rock energy," *Chinese Journal of Rock Mechanics and Engineering*, vol. 34, pp. 1–11, 2015.

[37] J. Cho, P. Martin, and L. W. Poon, "The older they are, the less successful they become? Findings from the Georgia Centenarian Study," *Journal of Aging Research*, vol. 2012, Article ID 695854, 8 pages, 2012.

[38] Itasca Consulting Group Inc, *FLAC3D 5.0 Manual*, ICG, Minneapolis, 2010.

[39] H. Kang, J. Lin, X. Zhang, and Y. Wu, "In-situ stress measurements and distribution laws in Lu'an underground coal mines," *Rock and Soil Mechanics*, vol. 31, no. 3, pp. 827–831, 2010.

[40] M. Wang, Z. Song, D. Zheng, W. Shen, P. Gou, and S. Wei, "FLAC^{3D} in the development and application of energy dissipation of rock model," *Journal of coal*, vol. 46, no. 8, pp. 2565–2573, 2021.

[41] S. Cicek, I. B. Tulu, M. V. Dyke, T. Klemetti, and J. Wickline, "Application of the coal mine floor rating (CMFR) to assess the floor stability in a central Appalachian coal mine," *International Journal of Mining Science and Technology*, vol. 31, no. 1, pp. 83–89, 2021.